Article

Moore–Gibson–Thompson Stability Model in a Two-Temperature Photonic Semiconductor Excited Medium Affected by Rotation and Initial Stress

Riadh Chteoui [1,2], Kh. Lotfy [3,*], M. A. Seddeek [4], A. El-Dali [4,5,6] and W. S. Hassanin [4]

[1] Lab. of Algebra, Number Theory and Nonlinear Analysis, Department of Mathematics, Faculty of Sciences, University of Monastir, Monastir 5019, Tunisia

[2] Department of Mathematics, Faculty of Sciences, University of Tabuk, Tabuk 47512, Saudi Arabia

[3] Faculty of Science, Department of Mathematics, Zagazig University, Zagazig P.O. Box 44519, Egypt

[4] Faculty of Science, Department of Mathematics, Helwan University, Cairo P.O. Box 11795, Egypt

[5] Future University, New Cairo 11835, Egypt

[6] Department of Information System, Higher Institute for Computer Science, El-Shorouk Academy, Cairo 4920213, Egypt

[*] Correspondence: khlotfy@zu.edu.eg

Abstract: In this paper, the two-temperature theory is used to examine a novel model that generalizes the Moore–Gibson–Thompson (MGT) effect according to two-dimensional electronic/thermoelastic deformation. The main equations for a semiconductor medium in the context of the impact of rotation are explained in terms of the impact of the initial hydrostatic stress at the free surface. The normal-mode approach is used to derive the precise formulae for the fundamental physical quantities (i.e., normal displacement, normal load stress, electronic diffusion (carrier density), dynamic and conductive temperature distribution) under the influence of the two-temperature coefficient. The comparison with the base state is performed using linear stability analysis. To make some comparisons based on the various values of thermal memories, the influence of a number of novel parameters is applied to each of our primary physical quantities, such as the rotation parameter and the initial stress. An example of the main fields' perturbation is also obtained and graphically described.

Keywords: rotation; Moore–Gibson–Thompson; photothermal; stability; harmonic wave; two-temperature

1. Introduction

Through the multiple studies of materials science, the importance of studies that are conducted on semiconductors has been demonstrated. Semiconductors in recent studies have shown many important applications in modern industries such as aircraft, electronics, and sensors, as well as in the production of electrical energy from clean sources such as the Sun. While semiconductors have unique properties among newly discovered materials, they include materials that are not completely insulating—such as reinforced plastic—or highly conductive materials such as copper. However, these substances undergo what is known as photothermal excitation when they are subjected to sunshine, a laser beam, or other light sources. In semiconductors, the movement of the electric current is caused by the plasma, which is formed when internal electrons are internally excited by a rise in temperature and migrate quickly to the surface. This preceding process is known as electronic deformation (ED) of semiconductors. On the other hand, it is accompanied by another blinding inside the material caused by internal particle collisions, which is known as thermoelastic deformation (TED). The structural framework used to analyze semiconductors is photo-thermoelasticity, which describes the interactions between electron diffusion, thermal deformation, and elastic deformation. Technologies for renewable energy are being developed using semiconductors and photothermal theory.

Boit [1] presented the first theory of coupled thermoelasticity to resolve the inconsistency in the idea of uncoupled thermoelasticity. The traditional Fourier heat conduction rule serves as the foundation for the conventional dynamic theory of thermoelasticity (CD theory). Because the resulting governing equation is parabolic in form, this theory assumes that a thermal signal can travel at an unlimited speed. The standard thermoelastic model, however, is physically unacceptable in some situations—such as a short-pulse laser heating process, or under working settings for low temperatures—because the thermal conditions cannot reach equilibrium during the brief work time. Therefore, it is more appropriate to utilize an extended hyperbolic thermoelastic model to simulate these problems, since this acknowledges that the thermal signal propagates at a finite speed. Many researchers are familiar with and have conducted numerous studies using the Lord–Shulman (LS) model [2], which has one relaxation period, and the Green–Lindsay (GL) model [3], which has two relaxation times [4–6].

Gordon et al. [7] discovered an interactive sample that contains a photothermal lens (a laser-based device that produces photothermal blooming), which led to the development of the first photothermal technique. Later, Kreuzer [8] demonstrated that the use of laser light sources allowed photoacoustic spectroscopy to be employed for the investigation of sensitive materials. Measurements of thermal diffusivities, velocities of sound, bulk flow velocities, surface thicknesses, and specific heats have all been subsequently carried out using photothermal methods [9–12]. Modeling the complicated systems through simultaneous analysis of the associated plasma, thermal, and elastic wave equations constitutes a general theoretical description of the TED and ED effects in semiconducting materials during photothermal processes [13]. Several theoretical methods have been used to analyze the connections between photothermal and thermoelastic equations. It is conceivable to comprehend the physical properties of elastic semiconductor materials by using unique methods that include modernized phase-lag techniques.

Chen et al. [14–16] presented a new theory of heat conduction in a deformed body that describes a two distinct temperatures: the conductive temperature and the thermodynamic temperature. According to Chen et al. [16], the difference between these two temperatures is related to the amount of heat available. The two different temperatures are the same in a time-independent situation when there is no heat source present. However, there is a general difference between the two temperatures in time-dependent situations—particularly for issues with wave propagation—regardless of the heat source. The results obtained from using two-temperature thermoelasticity with multiple relaxation durations were later examined by Youssef et al. [17–19], who demonstrated that they are qualitatively different from those obtained when using one-temperature thermoelasticity. Quintanilla and Tien [20] described the current stability of structural behavior, spatial behavior, and two-temperature thermoelastic convergence.

Given the wide range of potential uses for high-intensity ultrasound in both medical and industrial settings—including lithotripsy, heat therapy, ultrasound cleaning, and more—it is not unexpected that many studies have been conducted [21]. The Moore–Gibson–Thompson equation has been used to simulate high-amplitude sound vibrations. A lot of scientific research has been carried out recently on the MGT equation. There is excessive consideration of fluid mechanics in this theory because it was derived using a third-order differential equation. Quintanilla [22,23] developed an original thermoelastic MGT heat transfer theory. The relaxation factor for the suggested new heat equation was added to GN-III using the energy equation of Abouelregal et al. [24,25]. The thermoelasticity theory was examined by Marin et al. [26] in the context of the MGT model's initial values as determined by the dipolar elastic feature. However, the modified Green–Naghdi (GN) III model was used to study the behavior mechanisms of thermo-optical waves according to a rotating field of an elastic semiconductor medium [27]. When the thermoelasticity theory and a high-intensity ultrasonic effect are employed using the MGT model, the variety of applications increases greatly, as seen recently [28]. Lotfy et al. [29] presented stable analytical solutions for the MGT model using a thermoelastic semiconductor excited medium.

The transient evaluation of elastic semiconductor materials exposed to thermal and optical plasma-imposed stress, as well as the stability of materials under the effects of rotation and initial stress, has not been studied, according to a review of the literature. In this paper, the two-temperature problem is investigated for a semiconducting material during a photothermal MGT process in a two-dimensional free surface deformation under the influence of mechanical force. In this phenomenon, the exact formulations of physical quantities with two temperature parameters under the influence of rotation and initial tension are obtained using the harmonic wave approach. The steady-field cases are obtained by the addition of an infinitesimal disturbance to the main dynamic variables in the elastic semiconductor to study the stability.

2. The Problem Description and the Basic Governing Equations

When the medium is in a rotating uniform case with an angular velocity $\Omega = \Omega n$ (where n is a unit vector taken in the direction of the rotation axis), in this case, the motion equation has a two additional terms, as follows:

(1) $\Omega \times (\Omega \times u)$, due to time-varying motion only.
(2) $2\Omega \times \dot{u}$, u is the displacement vector.

The equations of coupled plasma and thermal motion in this case according to the generalized MGT model take the following form:

$$\left. \begin{array}{l} \rho[\ddot{u}_i + \{\Omega \times (\Omega \times u)_i\} + \{2\Omega \times \dot{u})_i\}] = \\ \sigma_{ij,j} = (\mu - \tfrac{p}{2})\nabla^2 \vec{u}(\vec{r},t) + (\mu + \lambda - \tfrac{p}{2})\nabla(\nabla.\vec{u}(\vec{r},t) - \gamma\nabla T(\vec{r},t) - \gamma_n\nabla N(\vec{r},t) \end{array} \right\} \quad (1)$$

The focused variable quantities are $N(\vec{r},t)$, σ_{ij}, and $T(\vec{r},t)$, which are defined as the carrier intensity (density), stress tensor, and temperature distribution, respectively (where $\vec{r}$ is the position vector). The main fields are stated in the xz plane with the time variable t and initial stress p for the linear, homogenous, and isotropic semiconductor medium.

The link between plasma and thermal distribution can be introduced as follows [30,31]:

$$\frac{\partial N}{\partial t} = D_e \nabla^2 N - \frac{N}{\tau} + \kappa T \quad (2)$$

where $\kappa = \frac{\partial N_0}{\partial T}\frac{T}{t}$ is a coupling parameter with thermal activation, and N_0 is the equilibrium carrier concentration at normal temperature.

The heat flux during thermal conductivity can be defined in terms of temperature gradient as the following relationship, in accordance with Fourier's classical law of heat conductivity:

$$q = -k\nabla\varphi \quad (3)$$

The heat equation is as follows:

$$\rho C_e \frac{\partial T(\vec{r},t)}{\partial t} = k\nabla^2\varphi(\vec{r},t) - \frac{E_g}{\tau}N(\vec{r},t) - \gamma T_0\nabla.\frac{\partial \vec{u}(\vec{r},t)}{\partial t} \quad (4)$$

where C_e denotes the specific heat of the exciting material. The most popular theory is that of Maxwell and Cattaneo, which modifies the Fourier law utilizing a constitutive equation involving the positive relaxation time τ_0, as follows [28]:

$$\left(1 + \tau_0\frac{\partial}{\partial t}\right)q = -k\nabla\varphi \quad (5)$$

Green and Naghdi [29] provide a novel model (GN-III) for heat conduction, which has the following constitutive equation:

$$q = -[k\nabla\varphi + k^*\nabla v] \quad (6)$$

where v is the thermal displacement, $\dot{v} = T$, and k^* is the rate of the thermal conductivity. However, the simplified heat conduction equation can be rewritten using the thermal memory as follows [27]:

$$(1 + \tau_0 \frac{\partial}{\partial t})q = -k\nabla\varphi - k^*\nabla v \tag{7}$$

According to the generalized Moore–Gibson–Thompson theory of photothermoelasticity (MGTPTE), Equations (5) and (7) can be used to derive the general heat conduction equation in the context of the two-temperature theory, which is expressed as follows [32]:

$$(1 + \tau_0 \frac{\partial}{\partial t})(\rho c_E \frac{\partial^2 T}{\partial t^2} + \gamma_\theta T_0 \ddot{e} - \frac{E_g}{\tau}\frac{\partial N}{\partial t}) = [k\nabla^2\dot{\varphi} + k^*\nabla^2\varphi] \tag{8}$$

The MGTPTE theory is the generalization form of the LS theory and the type III GN theory (GN-III).

The constants E_g, (μ, λ), D_E, τ, ρ, k, and T_0 represent the semiconductor energy gap, Lame's elastic constants, the carrier diffusion coefficient, the carrier lifetime, the density, and the semiconductor's thermal conductivity respectively. On the other hand, the volume of thermal expansion is $\gamma_\theta = (3\lambda + 2\mu)\alpha_t$, where α_t expresses the coefficient of thermal expansion, $\gamma_n = (3\lambda + 2\mu)d_n$, d_n is the ED coefficient, and δ_{ij} represents the Kronecker delta. In the xz plane, the displacement vector can be chosen as $\vec{u} = (u, 0, w)$, where the components are $u(x, z, t)$ and $w(x, z, t)$ with the strain $e = u_x + w_z$. According to the two-temperature theory with the positive two-temperature parameter α, the relationship between conduction temperature φ and the dynamic temperature T can be given as follows:

$$\varphi - T = \alpha\left(\frac{\partial^2}{\partial x^2} + \frac{\partial^2}{\partial z^2}\right)\varphi \tag{9}$$

In the case of $\alpha = 0$, the one-temperature theory is obtained, where $\varphi = T$. When the body forces absence, the constitutive equations under the influence of initial stress are as follows:

$$\sigma_{xx} = (2\mu + \lambda)\frac{\partial u}{\partial x} + \lambda\frac{\partial w}{\partial z} - (2\mu + 3\lambda)(\gamma T + d_n N) - P \tag{10}$$

$$\sigma_{zz} = (2\mu + \lambda)\frac{\partial w}{\partial z} + \lambda\frac{\partial u}{\partial x} - (2\mu + 3\lambda)(\gamma T + d_n N) - P \tag{11}$$

$$\sigma_{xz} = s_1\frac{\partial u}{\partial z} + s_2\frac{\partial w}{\partial x} \tag{12}$$

where $s_1 = (\mu + \frac{P}{2})$, $s_2 = (\mu - \frac{P}{2})$.

3. Formulation of the Problem

According to the generalized MGTPTE, the equation can be rewritten in the 2D deformation under the effect of the rotational field with the influence of the initial hydrostatic stress in the following form:

$$\left.\begin{array}{l} \rho(\frac{\partial^2 u}{\partial t^2} - \Omega^2 u + 2\Omega\frac{\partial w}{\partial t}) = \\ (\lambda + 2\mu - \frac{P}{2})\frac{\partial^2 u}{\partial x^2} + (\mu - \frac{P}{2})\frac{\partial^2 u}{\partial z^2} + (\lambda + \mu - \frac{P}{2})\frac{\partial^2 w}{\partial x\partial z} - \gamma\frac{\partial T}{\partial x} - \gamma_n\frac{\partial N}{\partial x} \end{array}\right\} \tag{13}$$

$$\left.\begin{array}{l} \rho(\frac{\partial^2 w}{\partial t^2} - \Omega^2 w + 2\Omega\frac{\partial u}{\partial t}) = \\ (\lambda + 2\mu - \frac{P}{2})\frac{\partial^2 w}{\partial z^2} + (\mu - \frac{P}{2})\frac{\partial^2 w}{\partial x^2} + (\lambda + \mu - \frac{P}{2})\frac{\partial^2 u}{\partial x\partial z} - \gamma\frac{\partial T}{\partial x} - \gamma_n\frac{\partial N}{\partial x} \end{array}\right\} \tag{14}$$

The scalar and vector functions $\Pi(x, z, t)$ and $\psi(x, z, t)$ can be utilized in terms of the displacement components to further simplify the equation, which can be written in the following non-dimensional form:

$$u = \frac{\partial \Pi}{\partial x} + \frac{\partial \psi}{\partial z}, \quad w = \frac{\partial \Pi}{\partial z} - \frac{\partial \psi}{\partial x} \tag{15}$$

The following non-dimensional variables can be used for simplicity:

$$(x', z', u', w') = \frac{(x, z,, u, w)}{C_T t^*}, \ (T', \varphi') = \frac{\gamma(T, \varphi)}{(2\mu + \lambda - \frac{P}{2})}, \ N' = \frac{\gamma_n N}{(2\mu + \lambda - \frac{P}{2})}$$
$$\sigma' = \frac{\sigma}{\mu}, \ e' = e, \ (\Pi', \Psi') = \frac{(\Pi, \Psi)}{C_T^2 t^*}, P' = \frac{P}{\mu}, \ \Omega' = t^*\Omega, (t', \tau'_0) = \frac{(t, \tau_0)}{t^*} \tag{16}$$

Dropping the dashes and using Equation (15), the main equations can be rewritten in the following form:

$$(\nabla^2 - q_1 - q_2\frac{\partial}{\partial t})N + \varepsilon_3\, T = 0 \tag{17}$$

$$\left.\begin{array}{l}(k\frac{\partial}{\partial t} + k^*t^*)\nabla^2\varphi - \varepsilon_4(1 + \tau_0\frac{\partial}{\partial t})\frac{\partial^2 T}{\partial t^2} - \varepsilon_1(1 + \tau_0\frac{\partial}{\partial t})(\frac{\partial^2}{\partial t^2}\nabla^2\Pi) + \\ \varepsilon_2(1 + \tau_0\frac{\partial}{\partial t})\frac{\partial N}{\partial t} = 0\end{array}\right\} \tag{18}$$

$$(\nabla^2 + \Omega^2 - \frac{\partial^2}{\partial t^2})\Pi + 2\Omega\frac{\partial\Psi}{\partial t} - T - N = 0 \tag{19}$$

$$(\nabla^2 - \beta^2\frac{\partial^2}{\partial t^2} + \beta^2\Omega^2)\Psi - 2\beta^2\Omega\frac{\partial\Pi}{\partial t} = 0 \tag{20}$$

$$\varphi - T = \alpha\nabla^2\varphi \tag{21}$$

In the above equations, the main coefficients are

$$q_1 = \frac{kt^*}{D_E\rho\tau C_e}, \quad q_2 = \frac{k}{D_E\rho C_e}, \quad \varepsilon_1 = \frac{\gamma^2 t^* T_0}{k\rho}, \ \varepsilon_2 = \frac{\alpha_T E_g t^* k}{d_n\rho\tau C_e}, \ \varepsilon_3 = \frac{d_n k\kappa t^*}{\alpha_T\rho C_e D_E}$$
$$\varepsilon_4 = \rho\, C_e t^* C_T^2, \ \beta^2 = \frac{C_T^2}{C_L^2}, \ C_T^2 = \frac{2\mu + \lambda - \frac{P}{2}}{\rho}, \ C_L^2 = \frac{\mu - \frac{P}{2}}{\rho}, \gamma_n = (2\mu + 3\lambda)d_n, \tag{22}$$
$$t^* = \frac{k}{\rho C_e C_T^2}, \ \gamma = (2\mu + 3\lambda)\alpha_t$$

where the symbols ε_1, ε_2, and ε_3 refer to the thermoelasticity, the thermal energy, and the thermoelectric coupling parameters respectively. On the other hand, the non-dimensional stress component can be rewritten in the following form:

$$\sigma_{xx} = \frac{2\mu + \lambda}{\mu}\frac{\partial^2\Pi}{\partial x^2} + 2\frac{\partial^2\Psi}{\partial x\partial z} + \frac{\lambda}{\mu}\frac{\partial^2\Pi}{\partial z^2} - \frac{2\mu + \lambda}{\mu}(T + N) - P \tag{23}$$

$$\sigma_{zz} = \frac{2\mu + \lambda}{\mu}\frac{\partial^2\Pi}{\partial z^2} - 2\frac{\partial^2\Psi}{\partial x\partial z} + \frac{\lambda}{\mu}\frac{\partial^2\Pi}{\partial x^2} - \frac{2\mu + \lambda}{\mu}(T + N) - P \tag{24}$$

$$\sigma_{xz} = \frac{s_1}{\mu}\frac{\partial^2\Psi}{\partial z^2} + 2\frac{\partial^2\Pi}{\partial x\partial z} - \frac{s_2}{\mu}\frac{\partial^2\Psi}{\partial x^2} \tag{25}$$

4. The Solution of the Problem

The normal-mode approach, which is described as follows, can be used to solve Equations (17)–(21) for the physical variables:

$$[\Pi, \Psi, \varphi, T, \sigma_{ij}, N](x, z, t) = [\Pi^*(x), \Psi^*(x), \varphi^*(x), T^*(x), \sigma_{ij}^*(x), N^*(x)]\, e^{(\omega t + ibz)} \tag{26}$$

Equation (26) has the complex circular frequency ω and the imaginary unit $i = \sqrt{-1}$. On the other hand, the wave number is b in the z-direction, and the amplitudes of the main physical fields are Π^*, Ψ^*, φ^*, T^*, N^*, and σ_{ij}^*. Equations (17)–(21), which are defined by the normal-mode approach stated in Equation (26), have the following forms:

$$(D^2 - \alpha_1)N^* + \varepsilon_3\, T^* = 0 \tag{27}$$

$$\alpha_2(D^2 - b^2)\varphi^* - \alpha_3 T^* - \alpha_4(D^2 - b^2)\Pi^* + \alpha_5 N^* = 0 \tag{28}$$

$$(D^2 - \alpha_6)\Pi^* + \alpha_7\Psi^* - T^* - N^* = 0 \tag{29}$$

$$(D^2 - \alpha_8)\Psi^* - \alpha_9\Pi^* = 0 \tag{30}$$

$$(D^2 - A_1)\varphi^* + \beta^* T^* = 0 \tag{31}$$

The stress components also take the following forms:

$$\sigma_{xx}{}^* = V_1 D^2\Pi^* - V_2 b^2\Pi^* + 2ibD\Psi^* - V_1(T^* + N^*) \tag{32}$$

$$\sigma_{zz}{}^* = -V_1 b^2\Pi^* + V_2 D^2\Pi^* - 2ibD\Psi^* - V_1(T^* + N^*) \tag{33}$$

$$\sigma_{xz}{}^* = 2ibD\Pi^* - (V_3 D^2 + V_4 b^2)\Psi^* \tag{34}$$

The main quantities in the above system can be written as follows:

$$D = \tfrac{d}{dx},\ \alpha_1 = b^2 + q_1 + q_2,\ \alpha_2 = k\omega + k^*t^*,\ \alpha_3 = \varepsilon_4(1 + \tau_0\omega)\omega^2,\ \alpha_4 = \varepsilon_1(1 + \tau_0\omega)\omega^2,$$
$$\alpha_5 = \varepsilon_2(1 + \tau_0\omega)\omega,\ \alpha_6 = b^2 + \omega^2 - \Omega^2,\ \alpha_7 = 2\Omega\omega,\ \alpha_8 = b^2 + \beta^2\omega^2 - \beta^2\Omega^2,$$
$$\alpha_9 = 2\Omega\omega\beta^2\ A_1 = b^2 + \beta^*,\ \beta^* = \tfrac{1}{\alpha},\ V_1 = \tfrac{(2\mu+\lambda)}{\rho},\ V_2 = \tfrac{\lambda}{\mu},\ V_3 = \tfrac{s_2}{\mu},\ V_4 = \tfrac{s_1}{\mu},$$
$$V_5 = \alpha_6 + \alpha_8,\ V_6 = \alpha_6\alpha_8 + \alpha_7\alpha_9 \tag{35}$$

If—and only if—the factor matrix's determination vanishes, then the system of Equations (27)–(31) has a non-trivial solution, which can be represented as follows:

$$\begin{vmatrix} 0 & 0 & 0 & (D^2 - \alpha_1) & \varepsilon_3 \\ -\alpha_4(D^2 - b^2) & 0 & \alpha_2(D^2 - b^2) & \alpha_5 & -\alpha_3 \\ (D^2 - \alpha_6) & \alpha_7 & 0 & -1 & -1 \\ -\alpha_9 & (D^2 - \alpha_8) & 0 & 0 & 0 \\ 0 & 0 & (D^2 - A_1) & 0 & \beta^* \end{vmatrix} = 0 \tag{36}$$

Using an elimination method between Equations (27) and (31), we can derive the partial differential equation from the eighth order as follows:

$$\left[D^8 - ED^6 + FD^4 - GD^2 + H \right] T^*(x) = 0 \tag{37}$$

The principle coefficients of Equation (37) take the following form:

$$\left. \begin{aligned} E = \tfrac{1}{A_3}(&-\beta^* b^2\alpha_2 - \beta^*\alpha_1\alpha_2 - \beta^*\alpha_2\alpha_6 - \beta^*\alpha_2\alpha_8 - b^2\alpha_4 - A_1\alpha_3 - A_1\alpha_4 - \alpha_1\alpha_3 - \alpha_1\alpha_4 - \\ &\alpha_3\alpha_6 - \alpha_3\alpha_8 - \alpha_4\alpha_8 - \alpha_4\varepsilon_3 + \alpha_5\varepsilon_3) \end{aligned} \right\}, \tag{38}$$

$$\left. \begin{aligned} F = \tfrac{1}{A_3}(&b^2 A_1\alpha_4 + b^2\alpha_1\alpha_4 + b^2\alpha_4\alpha_8 + b^2\alpha_4\varepsilon_3 + A_1\alpha_1\alpha_3 + A_1\alpha_1\alpha_4 + A_1\alpha_3\alpha_6 + A_1\alpha_3\alpha_8 + \\ &A_1\alpha_4\alpha_8 + A_1\alpha_4\varepsilon_3 - A_1\alpha_5\varepsilon_3 + \alpha_1\alpha_3\alpha_6 + \alpha_1\alpha_3\alpha_8 + \alpha_1\alpha_4\alpha_8 + \alpha_3\alpha_6\alpha_8 + \alpha_3\alpha_7\alpha_9 + \alpha_4\alpha_8\varepsilon_3 - \\ &\alpha_5\alpha_6\varepsilon_3 - \alpha_5\alpha_8\varepsilon_3 + \beta^* b^2\alpha_1\alpha_2 + \beta^* b^2\alpha_2\alpha_6 + \beta^* b^2\alpha_2\alpha_8 + \beta^*\alpha_1\alpha_2\alpha_6 + \beta^*\alpha_1\alpha_2\alpha_8 + \\ &\beta^*\alpha_2\alpha_6\alpha_8 + \beta^*\alpha_2\alpha_7\alpha_9) \end{aligned} \right\}, \tag{39}$$

$$\left. \begin{aligned} G = \tfrac{1}{A_3}(&-\beta^* b^2\alpha_1\alpha_2\alpha_6 - \beta^* b^2\alpha_1\alpha_2\alpha_8 - \beta^* b^2\alpha_2\alpha_6\alpha_8 - \beta^* b^2\alpha_2\alpha_7\alpha_9 - \beta^*\alpha_1\alpha_2\alpha_6\alpha_8 - \\ &\beta^*\alpha_1\alpha_2\alpha_7\alpha_9 - b^2 A_1\alpha_1\alpha_4 - b^2 A_1\alpha_4\alpha_8 - b^2 A_1\alpha_4\varepsilon_3 - b^2\alpha_1\alpha_4\alpha_8 - b^2\alpha_4\alpha_8\varepsilon_3 - \\ &A_1\alpha_1\alpha_3\alpha_6 - A_1\alpha_1\alpha_3\alpha_8 - A_1\alpha_1\alpha_4\alpha_8 - A_1\alpha_3\alpha_6\alpha_8 - A_1\alpha_3\alpha_7\alpha_9 - A_1\alpha_4\alpha_8\varepsilon_3 + A_1\alpha_4\alpha_6\varepsilon_3 + \\ &A_1\alpha_5\alpha_8\varepsilon_3 - \alpha_1\alpha_3\alpha_6\alpha_8 - \alpha_1\alpha_3\alpha_7\alpha_9 + \alpha_5\alpha_6\alpha_8\alpha_3 + \alpha_5\alpha_7\alpha_9\alpha_3) \end{aligned} \right\}, \tag{40}$$

$$\left. \begin{aligned} H = \tfrac{1}{A_3}(&\beta^* b^2\alpha_1\alpha_2\alpha_6\alpha_8 + \beta^* b^2\alpha_1\alpha_2\alpha_7\alpha_9 + b^2 A_1\alpha_1\alpha_4\alpha_8 + \varepsilon_3\alpha_8\alpha_4 A_1 b^2 + A_1\alpha_1\alpha_3\alpha_6\alpha_8 \\ &+ A_1\alpha_1\alpha_3\alpha_7\alpha_9 - \varepsilon_3\alpha_8\alpha_6\alpha_5 A_1 - \varepsilon_3\alpha_9\alpha_7\alpha_5 A_1) \end{aligned} \right\}. \tag{41}$$

The factorization of the preceding Equation (37) is as follows:

$$(D^2 - k_1{}^2)(D^2 - k_2{}^2)(D^2 - k_3{}^2)(D^2 - k_4{}^2)\, T^* = 0. \tag{42}$$

where the roots of the following characteristic equation are $k_n{}^2 (n = 1, 2, 3, 4)$:

$$k^8 - Ek^6 + Fk^4 - Gk^2 + H = 0 \tag{43}$$

The solution of Equation (43) can be rewritten in a linear form when $x \to \infty$, as follows:

$$T^* = \sum_{n=1}^{4} M_n(b, \omega) \, e^{-k_n x} \tag{44}$$

Using the same method yields

$$\Pi^* = \sum_{n=1}^{4} H_{1n} M_n(b, \omega) \, e^{-k_n x}, \tag{45}$$

$$N^* = \sum_{n=1}^{4} H_{2n} M_n(b, \omega) \, e^{-k_n x}, \tag{46}$$

$$\varphi^* = \sum_{n=1}^{4} H_{3n} M_n(b, \omega) \, e^{-k_n x}, \tag{47}$$

$$\Psi^* = \sum_{n=1}^{4} H_{4n} M_n(b, \omega) \, e^{-k_n x}, \tag{48}$$

$$u^*(x) = D\Pi^* + ib\Psi^* = \sum_{n=1}^{4} M_n(b, \omega)_n (-H_{1n} k_n + ib \, H_{4n}) e^{-k_n x}, \tag{49}$$

$$w^*(x) = ib\Pi^* - D\Psi^* = \sum_{n=1}^{4} M_n(b, \omega)(ibH_{1n} + H_{4n} k_n) e^{-k_n x}. \tag{50}$$

where

$$H_{1n} = \frac{(k_n{}^2 - \alpha_1 - \varepsilon_3)(k_n{}^2 - \alpha_8)}{(k_n{}^2 - \alpha_1)(k_n{}^4 - V_5 k_n{}^2 + V_6)}, \tag{51}$$

$$H_{2n} = \frac{-\varepsilon_3}{(k_n{}^2 - \alpha_1)}, \tag{52}$$

$$H_{3n} = \frac{-\beta^*}{(k_n{}^2 - A_1)}, \tag{53}$$

$$H_{4n} = \frac{-\alpha_9 H_{1n}}{(k_n{}^2 - \alpha_8)}. \tag{54}$$

where $M_n (n = 1, 2, 3, 4)$ are some parameters depending on b and ω. On the other hand, the stress components can be rewritten in terms of M_n as follows:

$$\sigma^*{}_{xx} = \sum_{n=1}^{4} h_n M_n(b, \omega) \, e^{-k_n x}, \tag{55}$$

$$\sigma^*{}_{zz} = \sum_{n=1}^{4} h'_n M_n(b, \omega) \, e^{-k_n x}, \tag{56}$$

$$\sigma^*{}_{xz} = \sum_{n=1}^{4} h''_n M_n(b, \omega) \, e^{-k_n x}, \tag{57}$$

where

$$h_n = H_{1n}(V_1 k_n{}^2 - V_2 b^2) - 2ibk_n H_{4n} - V_1(1 + H_{2n}), \tag{58}$$

$$h_n{}' = -H_{1n}(V_1 b^2 - V_2 k_n{}^2) + 2ibk_n H_{4n} - V_1(1 + H_{2n}), \tag{59}$$

$$h_n'' = -2ibk_n H_{1n} - (V_3 k_n^2 + V_4 b^2) H_{4n}. \tag{60}$$

5. Boundary Conditions

The parameters M_n are determined in this section. In the physical problem, we should suppress the positive exponentials that are unbounded at infinity. The variables M_1, M_2, M_3, M_4 must be selected so that the surface boundary conditions at $x = 0$ (assuming the boundary is adjacent to the vacuum) have the following form:

The traction load on the half-space is the first mechanical normal boundary condition and has the following form:

$$\sigma_{xx}(0, z, t) = -p_1 e^{(\omega t + ibz)}. \tag{61}$$

Having no traction on the half-surface space is the second mechanical boundary condition:

$$\sigma_{xz}(0, z, t) = 0. \tag{62}$$

The isothermal condition at the boundary $x = 0$ is thermally insulated:

$$\frac{\partial T(0, z, t)}{\partial x} = 0. \tag{63}$$

The carriers have a limited chance of recombining when they reach the sample's surface during the diffusion process. Therefore, the carrier density's boundary condition can be as follows:

$$\frac{\partial N(0, z, t)}{\partial x} = \frac{s}{D_E} N. \tag{64}$$

The following equations can be obtained by substituting the expressions of the variables taken into consideration into the boundary conditions above:

$$\sum_{n=1}^{4} h_n M_n(b, \omega) = -p_1, \tag{65}$$

$$\sum_{n=1}^{4} h_n'' M_n(b, \omega) = 0, \tag{66}$$

$$\sum_{n=1}^{4} k_n M_n(b, \omega) = 0, \tag{67}$$

$$\sum_{n=1}^{4} k_n H_{2n} M_n(b, \omega) = \frac{-s}{D_E} N. \tag{68}$$

To determine the values of the four constants of M_n, a set of four equations is derived by using the boundary conditions (65)–(68) at the plate's surface $x = 0$. These constant values are obtained by applying the matrix's inverse method. As a result, we can deduce the plate's physical quantity expressions.

6. Stability

6.1. The Base State

The system of Equations (17)–(21) has a steady solution $\overline{N}_b(x)$, $\overline{\phi}_b(x)$, $\overline{\Pi}_b(x)$, $\overline{\psi}_b(x)$, and $\overline{T}_b(x)$, respectively, featuring a uniform longitudinal quantity expansion flow extension depending only on the horizontal direction x, without time. For this basic solution, the equations are reduced to

$$\frac{d^2 \overline{N}_b(x)}{dx^2} - q_1 \overline{N}_b(x) + \varepsilon_3 \overline{T}_b(x) = 0, \tag{69}$$

$$\frac{d^2\overline{\varphi}_b(x)}{dx^2} = 0, \tag{70}$$

$$\frac{d^2\overline{\Pi}_b(x)}{dx^2} + \Omega^2\overline{\Pi}_b(x) - \overline{T}_b(x) - \overline{N}_b(x) = 0, \tag{71}$$

$$\frac{d^2\overline{\Psi}_b(x)}{dx^2} + \beta^2\Omega^2\overline{\Psi}_b(x) = 0, \tag{72}$$

$$\overline{\varphi}_b(x) - \overline{T}_b(x) = \alpha\frac{d^2\overline{\varphi}_b(x)}{dx^2}. \tag{73}$$

On the other hand, the boundary conditions corresponding to the basic stress components and temperature gradient at $x = 0$ are as follows:

$$\frac{d^2\overline{\Pi}_b(x)}{dx^2} - (\overline{T}_b + \overline{N}_b) = \frac{p-p_1}{2\mu+\lambda}\mu, \quad \frac{d^2\overline{\Psi}_b}{dx^2} = 0, \quad \frac{d^2\overline{T}_b}{dx^2} = 0, \quad \frac{d\overline{N}_b}{dx} = \frac{s}{p_e}\overline{N}_{0b}. \tag{74}$$

The base state whose stability is of interest in this study is obtained by solving Equations (69)–(73) for the steady unidirectional media extension in the x-direction due to the uniform temperature gradient, rotation, and uniform carrier intensity, as follows:

$$\overline{\varphi}_b(x) = \varphi'_0\, x + \varphi_0, \tag{75}$$

$$\overline{\Psi}_b(x) = \frac{\Psi_1\,\sin[\beta\,\Omega(1+x)] + \Psi_{-1}\sin[\beta\,\Omega(1-x)]}{\sin(2\beta\,\Omega)}, \tag{76}$$

$$\overline{T}_b(x) = T'_0\, x + T_0, \tag{77}$$

$$\overline{N}_b(x) = \frac{\varepsilon_3\,\varphi_0}{q_1}[1 + \frac{s}{p_e\,q_1}\sinh(\sqrt{q_1}\,x)], \tag{78}$$

$$\left.\begin{array}{l} \overline{\Pi}_b(x) = \sin(\Omega\,x) + \frac{\varphi_0}{\Omega^2}(1 + \frac{\varepsilon_3}{q_1}) - \frac{1}{\Omega^2}(\varphi_0 + \frac{\varepsilon_3\,\varphi_0}{q_1} + \frac{p-p_1}{2\mu+\lambda}\mu) + \\[2mm] \frac{\varepsilon_3\,\varphi_0\,s}{p_e\,q_1^{\frac{3}{2}}(q_1+\Omega^2)}\sinh(\sqrt{q_1}\,x) \end{array}\right\}, \tag{79}$$

where $\Psi_1 = \Psi(x = 1)$, $\Psi_{-1} = \Psi(x = -1)$.

6.2. Linear Stability Analysis

This section considers the effects of superimposing an infinitesimal disturbance on the steady fields and other dynamic variables in a solid semiconductor plate that is similarly perturbed. We assume that the superimposed infinitesimal disturbances N', φ', Π', Ψ', T' are conjugated to $\overline{N}_b(x)$, $\overline{\phi}_b(x)$, $\overline{\Pi}_b(x)$, $\overline{\psi}_b(x)$, and $\overline{T}_b(x)$, respectively, which can be written as follows:

$$\Pi = \Pi' + \overline{\Pi}_b, \tag{80}$$

$$\Psi = \Psi' + \overline{\Psi}_b, \tag{81}$$

$$\varphi = \varphi' + \overline{\varphi}_b, \tag{82}$$

$$T = T' + \overline{T}, \tag{83}$$

$$N = N' + \overline{N}_b. \tag{84}$$

To determine how these slight disturbances to the base state evolved, a temporal linear stability analysis was used. The following describes how the perturbation quantities were expanded into Fourier modes in the z-direction with an exponential time dependence:

$$\varphi'(x,z,t) = \widetilde{\varphi}(x)\,e^{(\omega t+ibz)}, \tag{85}$$

$$\Psi'(x,z,t) = \widetilde{\Psi}(x)\,e^{(\omega t+ikz)}, \tag{86}$$

$$T'(x,z,t) = \widetilde{T}(x)\,e^{(\omega t+ikz)}, \tag{87}$$

$$N'(x, z, t) = \widetilde{N}(x) e^{(\omega t + ikz)}, \tag{88}$$

$$\Pi'(x, z, t) = \widetilde{\Pi}(x) e^{(\omega t + ikz)}. \tag{89}$$

In this case, Equations (17)–(21) can be rewritten in the following form:

$$\frac{d^2\widetilde{N}(x)}{dx^2} - [k^2 - q_1 - q_2\omega]\widetilde{N}(x) + \varepsilon_3\widetilde{T}(x) = 0, \tag{90}$$

$$\left. \begin{array}{c} (k\omega + k^*t^*)(\frac{d^2\widetilde{\varphi}(x)}{dx^2} - k^2\widetilde{\varphi}(x)) - \varepsilon_4(1 + \tau_0\omega)\omega^2\widetilde{T}(x) - \varepsilon_1(\omega^2 + \tau_0\omega^3)[\frac{d^2\widetilde{\Pi}(x)}{dx^2} - \\ k^2\widetilde{\Pi}(x)] + \varepsilon_2(1 + \tau_0\omega)\omega\widetilde{N}(x) = 0 \end{array} \right\}, \tag{91}$$

$$\frac{d^2\widetilde{\Pi}(x)}{dx^2} + [\Omega^2 - k^2 - \omega^2]\widetilde{\Pi}(x) + 2\Omega\omega\widetilde{\Psi}(x) - \widetilde{T}(x) - \widetilde{N}(x) = 0, \tag{92}$$

$$\frac{d^2\widetilde{\Psi}(x)}{dx^2} + [\beta^2(\Omega^2 - \omega^2) - k^2]\widetilde{\Psi}(x) - 2\beta^2\Omega\omega\widetilde{\Pi}(x) = 0, \tag{93}$$

$$\widetilde{T}(x) = (k^2\alpha - 1)\widetilde{\varphi}(x) - \alpha\frac{d^2\widetilde{\varphi}(x)}{dx^2}. \tag{94}$$

The boundary conditions can be represented as follows:

$$\frac{2\mu + \lambda}{\mu}\frac{d^2\widetilde{\Pi}(0)}{dx^2} + 2ik\frac{d\widetilde{\Psi}(0)}{dx} - \frac{\lambda k^2}{\mu}\widetilde{\Pi}(0) - \frac{2\mu + \lambda}{\mu}[\widetilde{T}(0) + \widetilde{N}(0)] + R = 0, \tag{95}$$

$$\frac{s_1 k^2}{\mu}\widetilde{\Psi}(0) - 2ik\frac{d\widetilde{\Pi}(0)}{dx} + \frac{s_2}{\mu}\frac{d^2\widetilde{\Psi}(0)}{dx^2} = 0, \tag{96}$$

$$\frac{d\widetilde{T}(0)}{dx} = 0, \quad \frac{d\widetilde{N}(0)}{dx} = \frac{s}{p_e}\widetilde{N}_0(0). \tag{97}$$

Equations (90)–(94) with boundary conditions (95)–(97) are the basic equations for the linear stability analyses.

7. Numerical Results and Discussions

Consider a numerical example for which the computational results are provided to numerically examine the mentioned problems. For numerical simulation, silicon (Si) is the material of choice as an example of a semiconductor. The problem's numerical constants (in SI units) are listed in Table 1 [33–35].

Table 1. The physical constants of the Si medium.

Unit	Symbol	Si	Unit	Symbol	Si
N/m^2	λ	3.64×10^{10}	N	p	100
N/m^2	μ	5.46×10^{10}	J/(kg K)	C_e	695
K	T_0	800	m/s	s	2
kg/m^3	ρ	2330	s	τ	5×10^{-5}
m^3	d_n	-9×10^{-31}	N	α	3.688×10^{-5}
m^2/s	D_E	2.5×10^{-3}	Nm^{-2}	ς_1	1.475×10^{10}
eV	E_g	1.11	K^{-1}	α_t	4.14×10^{-6}
Wm^{-1}K^{-1}	k	150	K^{-1}	α_t	4.14×10^{-6}

The numerical results discussed above were applied to the real part of the main physical field distributions in Figures 1–4 when the non-dimensional mechanical load was $p_1 = 1$ at $z = -1$, in the case where a short time was applied when $\omega = \omega_0 + i\xi$, $\omega_0 = -0.3$, $\xi = 0.1$ with the wave number $b = 0.9$. For a small dimensionless time, the exponential

function $e^{\omega t} = e^{\omega_0 t}(\cos \xi t + i \sin \xi t)$ when conducting the real analysis can be chosen as $\omega = \omega_0$ (real).
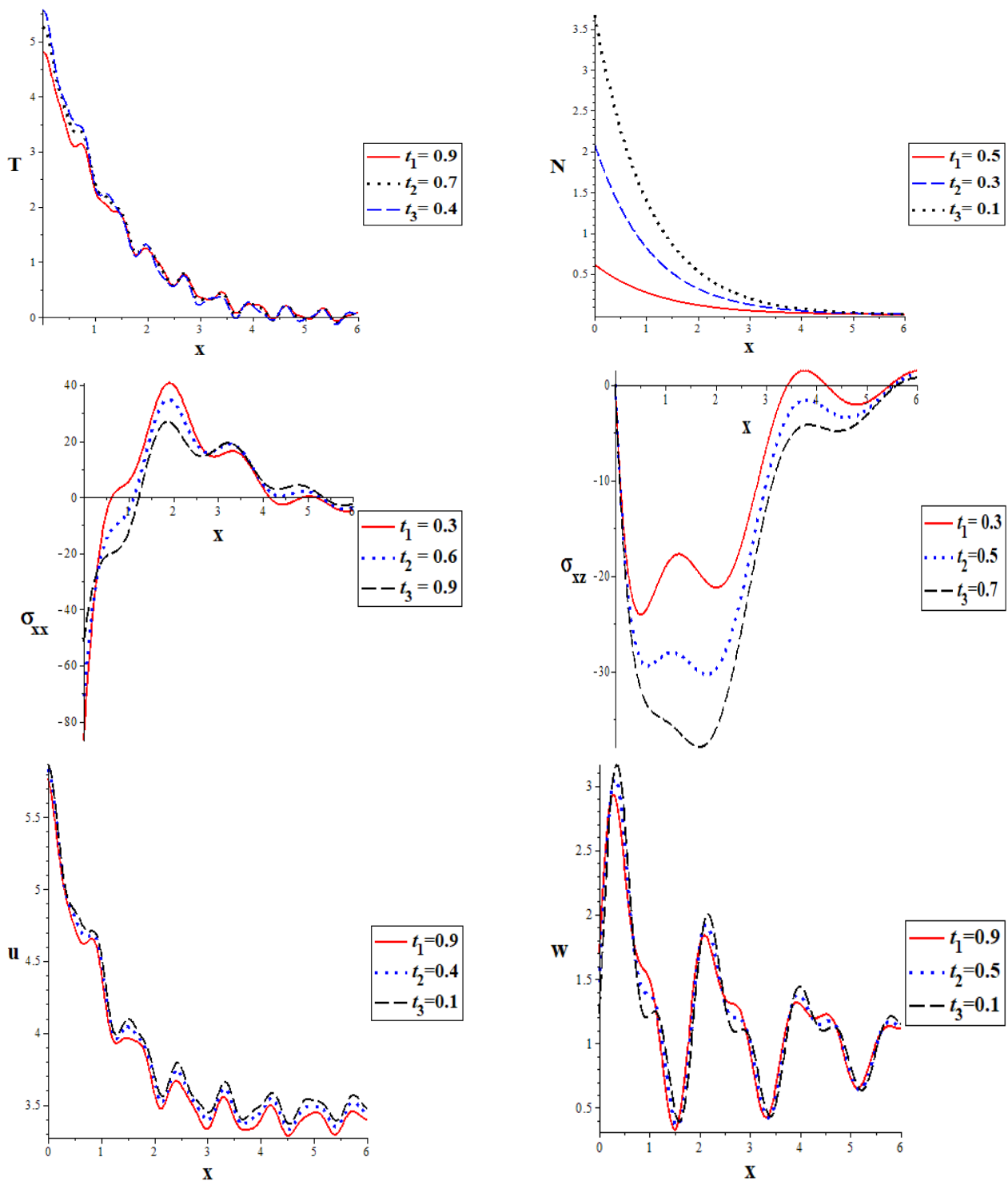

Figure 1. The main changes in the physical fields plotted against the horizontal distance for various short times in a rotational field and under initial hydrostatic stress.
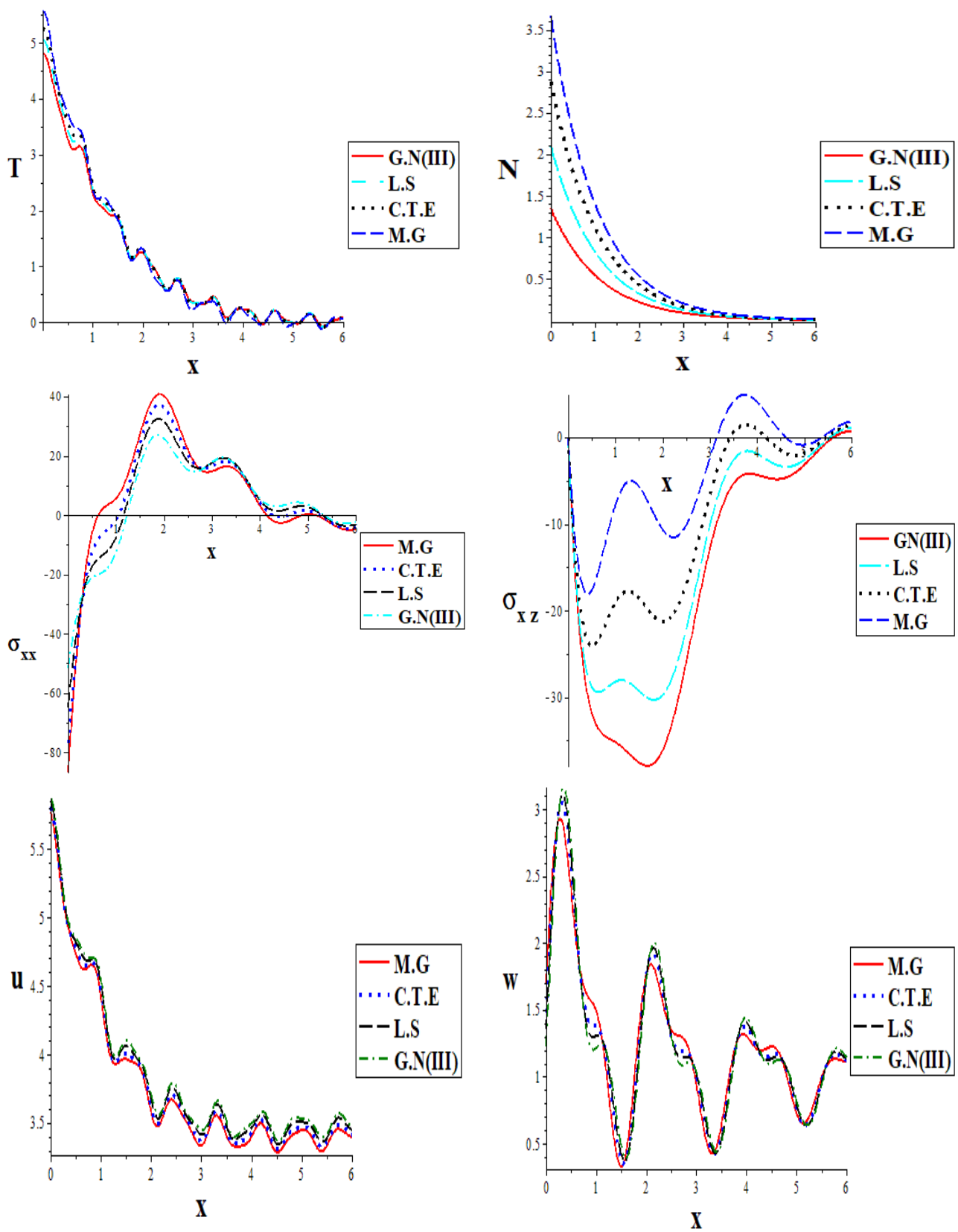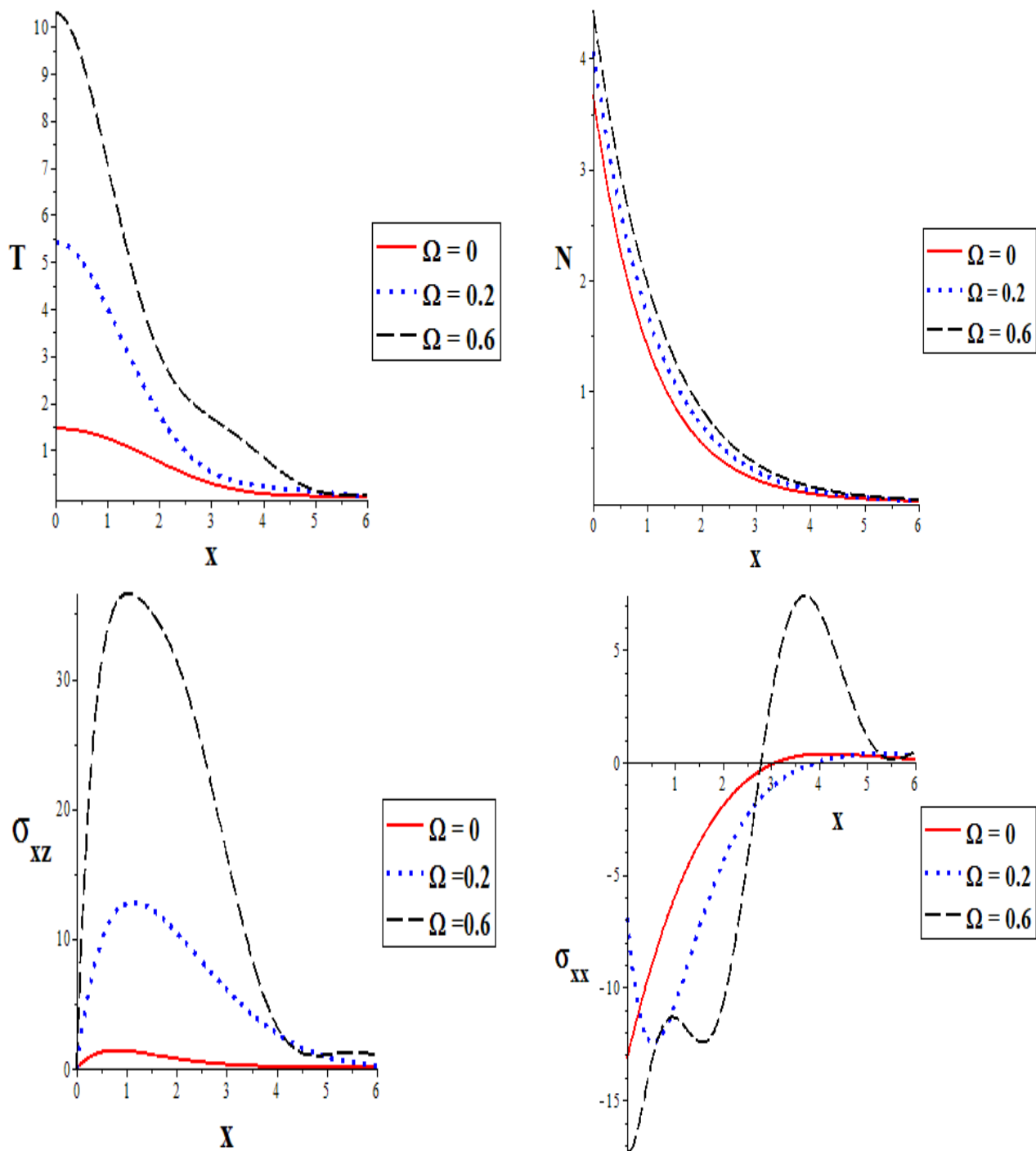
Figure 2. The main changes in the physical fields plotted against the horizontal distance for various photothermoelastic models in a rotational field and under initial hydrostatic stress when $t = 0.3$.

Figure 3. The main changes in the physical fields plotted against the horizontal distance for various small values of rotation parameters according to the MGT model in the presence of initial hydrostatic stress.
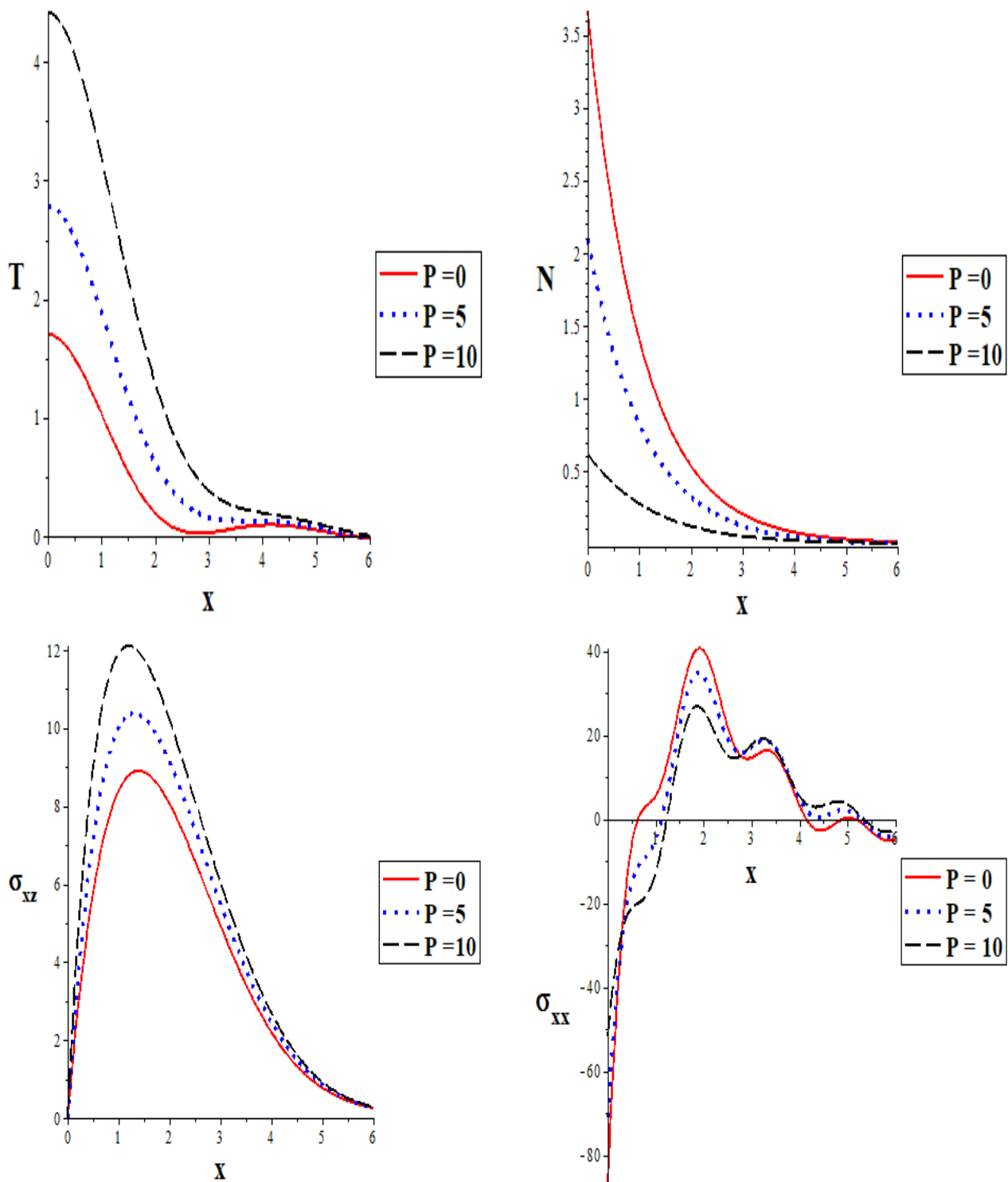
Figure 4. The main changes in the physical fields plotted against the horizontal distance for various values of initial hydrostatic stress in a rotational field according to the MGT model.

Figure 1 displays the influence of different values of time on the main quantities (which are shown in the subfigures) relative to the horizontal distance x. The numerical computations were calculated according to the Moore–Gibson–Thompson (MGT) model in a rotational field under the impact of the initial hydrostatic stress. According to this figure, the wave propagation distributions satisfy the surface conditions and reach zero (vanish) as x tends towards infinity. This behavior for the wave propagations is physically acceptable. The results observed in this work are consistent with the practical experiments reported in [36,37].

The numerical results in Figure 2 illustrate how the new MGT theory's predictions (including the MGT equation) differ from those of other photothermoelastic models under the impact of the rotational field and initial stress. Whereas the classical thermoelastic (CTE) model is obtained when k^* and τ_0 are zero, when $k^* = 0$ only, the Lord–Shulman (LS) model is attained; when $k = \tau_0 = 0$, the type II Green–Naghdi model (GN-II) is obtained; and when $\tau_0 = 0$, the type III Green–Naghdi model (GN-III) is obtained. It is evident from the results of the numerical analysis that the physical field values anticipated by the GN-III and CTE theories are significantly higher than those predicted by the MGT theory and other generalized models of photo-thermoelasticity. Furthermore, the generalized photo-thermoelastic model of GN-III converges with the classical photo-thermoelastic model (CTE), which does not break down under heat as quickly as other generalized thermoelastic theories. This demonstrates the limitations of the GN-III model which, like the conventional model, forecasts the dispersion of thermal waves at unrestricted speeds. The influence of the relaxation times is observed in all of the wave propagation behavior. This illustrates how precisely the proposed MGT model, which resolves the inconsistency in the GN-III photothermoelasticity model, works. The obtained results offer additional proof that, according to the LS, GN-II, and MGT theories, the values of various physical domains would converge and act similarly.

Figure 3 displays the influence of the rotation parameters on the main wave propagations of the main physical distributions with respect to the horizontal distance. The MGT model and the effect of the initial stress were used in numerical computations to investigate the physical wave propagation distributions. The obvious influences of the rotation parameters on the values of wave amplitudes are shown. The wave propagation behavior under study was significantly impacted by changes in the rotational parameters.

The impact of the initial hydrostatic stress on the main wave propagations of the principal physical distributions relative to the horizontal distance is shown in Figure 4. To explore the physical wave propagation distributions, numerical computations were conducted using the MGT model and the impact of the rotational field. We observed how the rotational parameters affect the values of the wave amplitudes. Changes in the initial stress parameters had a major impact on the investigated wave propagation behavior.

Figure 5A–D illustrate that, in contrast to the carrier intensity perturbation—which starts when $\overline{N}_{0b} = 0$—the rotation parameter disturbs the temperature and the stress components and shifts the σ_{xx} perturbation curves without any influence on the associated thresholds.
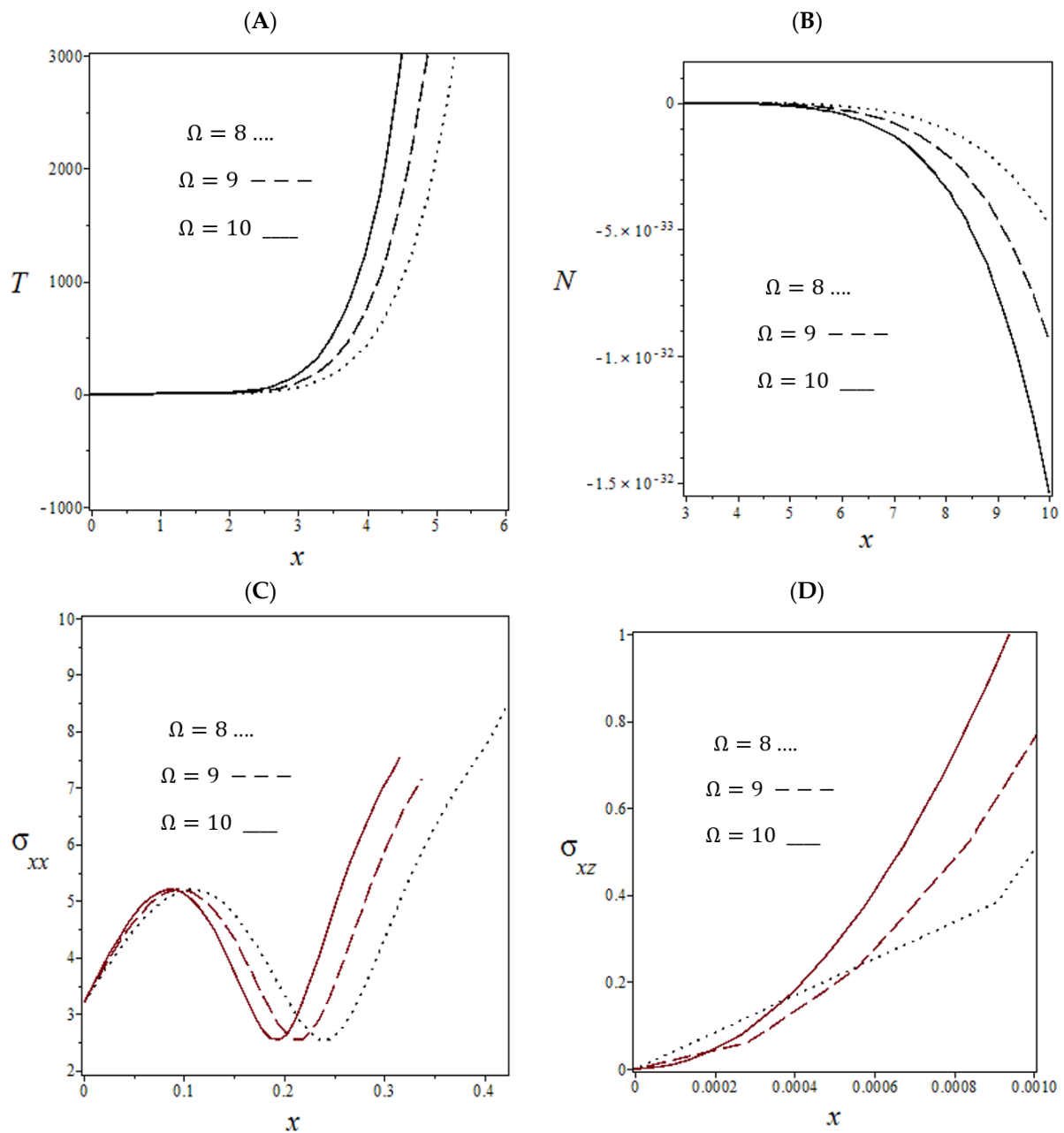
(A)

(B)

(C)

(D)

Figure 5. (**A–D**) Perturbation evolution for $T(x)$, $N(x)$, σ_{xx}, *and* σ_{xz} for the complex circular frequency $\omega_{min} = -0.258$ at $K_{max} = 0.25649$ (wave number) when $\varepsilon_3 = -7.234118786 \times 10^{-36}$ and with three small values of the rotation parameter Ω.

Figure 6A demonstrates the stabilizing effect of the large rotation parameter values ($\Omega = 10^4$, 10^5 and 10^6), especially for the large wave number values, where $b > 1$ (short waves). Figure 6B describes the effect of the small rotation parameter Ω on the stability behavior. The non-damping (destabilizing) effect for the long waves ($b \ll 1$) is small compared with that for the short waves. In Figure 6A,B, the complex circular frequency ω varies against the wave number ($b = K$, variable not constant) for different values of rotation parameters. On the other hand, the value of the complex circular frequency $\omega_{min} = -0.258$ and the value of the wave number $b_{max} = K_{max} = 0.25649$ are required for the medium to be stable [38–40].
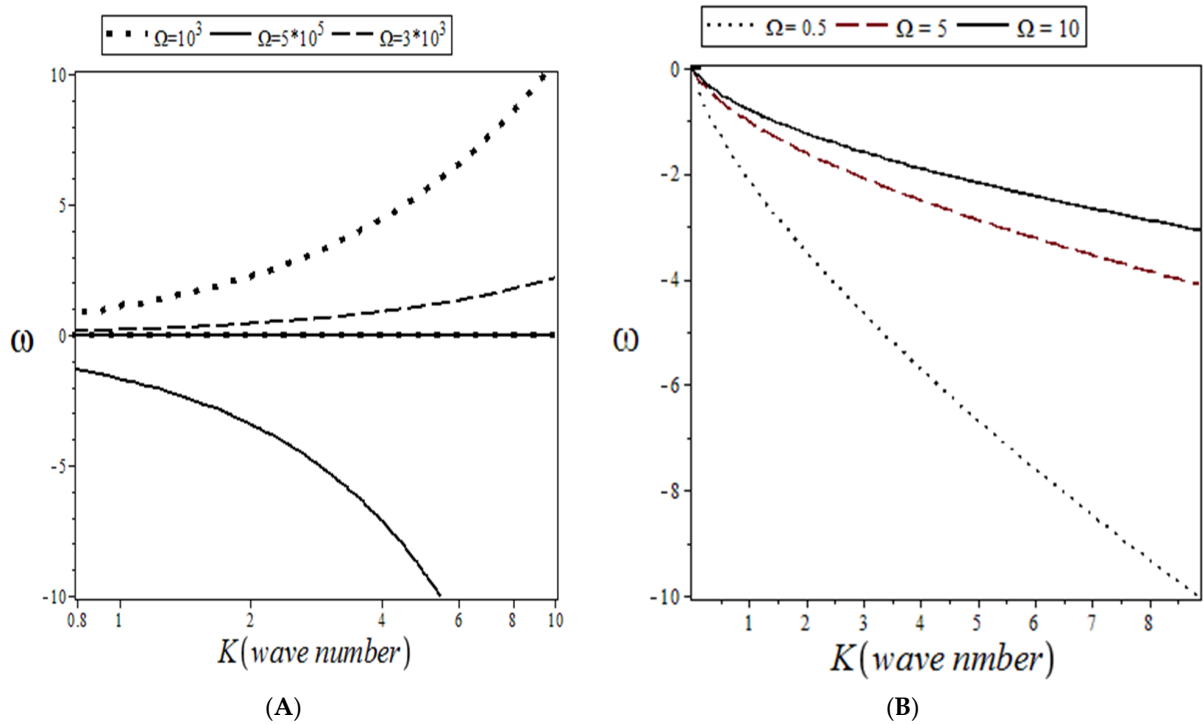
Figure 6. (**A**,**B**) Growth rate of the most dangerous mode as a function of the wave number b for $\varepsilon_3 = -7.234118786 \times 10^{-36}$ and different large and small values of the rotation parameter under initial hydrostatic stress according to the MGT model.

Figure 7 indicates the short-wavelength stability limit, where the growth rate decreases regularly when increasing the wave number $b = K$ (variable, from $K = 0$) and tends towards a minimum value ω ($\omega = -0.256410257$) when the wave number K becomes small ($b = 0.25641026$).
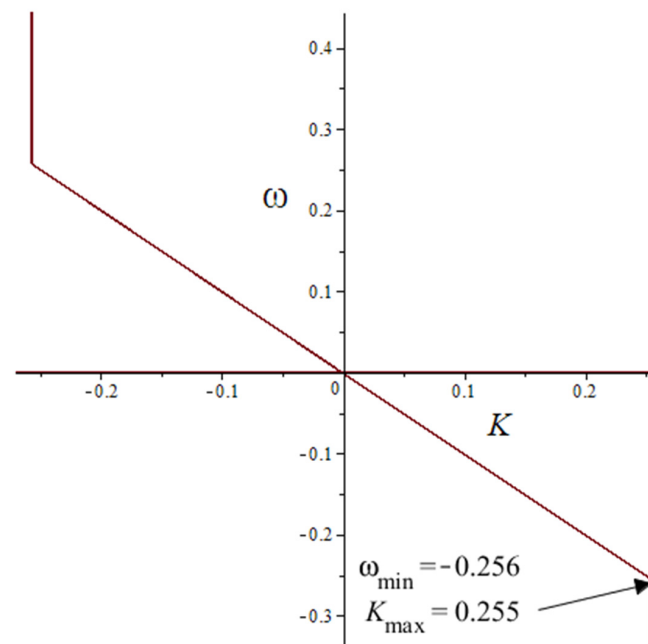

Figure 7. Minimum growth rate as a function of the wave number K for $\varepsilon_3 = -7.234118786 \times 10^{-36}$ in a rotational field $\Omega = 10$ with initial hydrostatic stress according to the MGT model.

Figure 8 explains the strong damping (i.e., stabilizing) effect of the small rotation parameter values for the first stability case, observed as the minimum negative growth rate $\omega = -0.258$ at $K = 0.25649$ ($K < 1$).
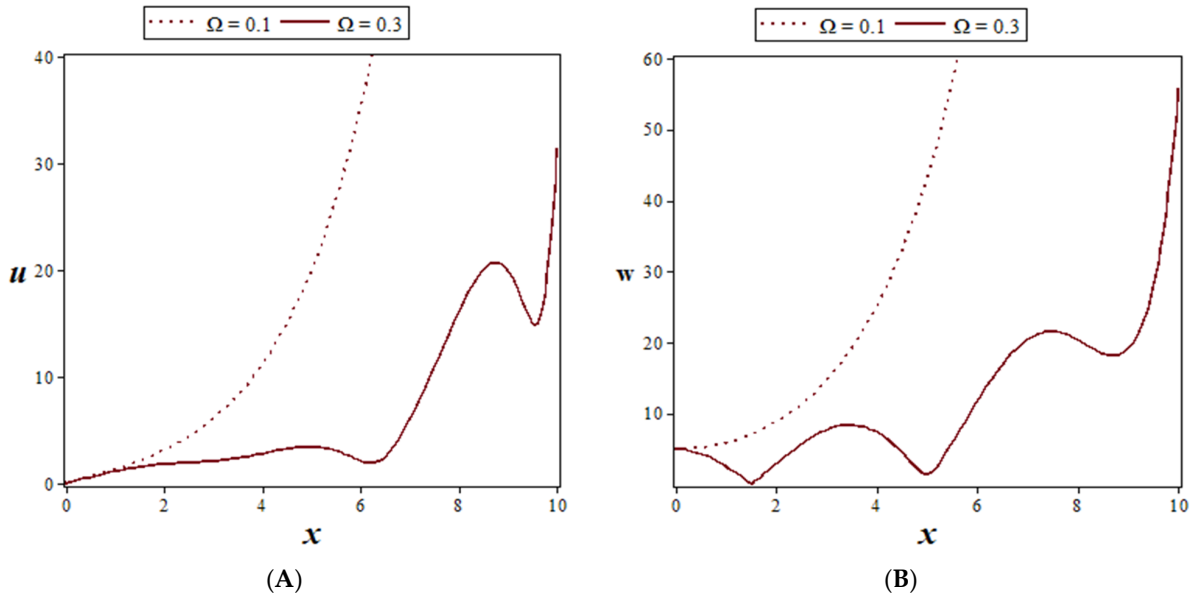

(A)　　　　　　　　　　　　　　　　　　　　　　　　　(B)

Figure 8. (**A**,**B**) Displacement components' perturbation $u(x)$ and $w(x)$ for the complex circular frequency $\omega_{min} = -0.258$ at $K_{max} = 0.25649$ (wave number) when $\varepsilon_3 = -7.234118786 \times 10^{-36}$ and with two small values of the rotation parameter Ω.

In Figure 9A, the two-dimensional neutral curve decreases regularly when increasing $b(b > 0.1)$ and tends towards a minimum value when the wave number b becomes large ($b = 10$ for the short wavelength). In Figure 9B, to construct the critical hypersurface in the parameter space (ε_3, Ω, b), sets of critical curves in the (ε_3, Ω) plane are computed for different values of the wave number [41].

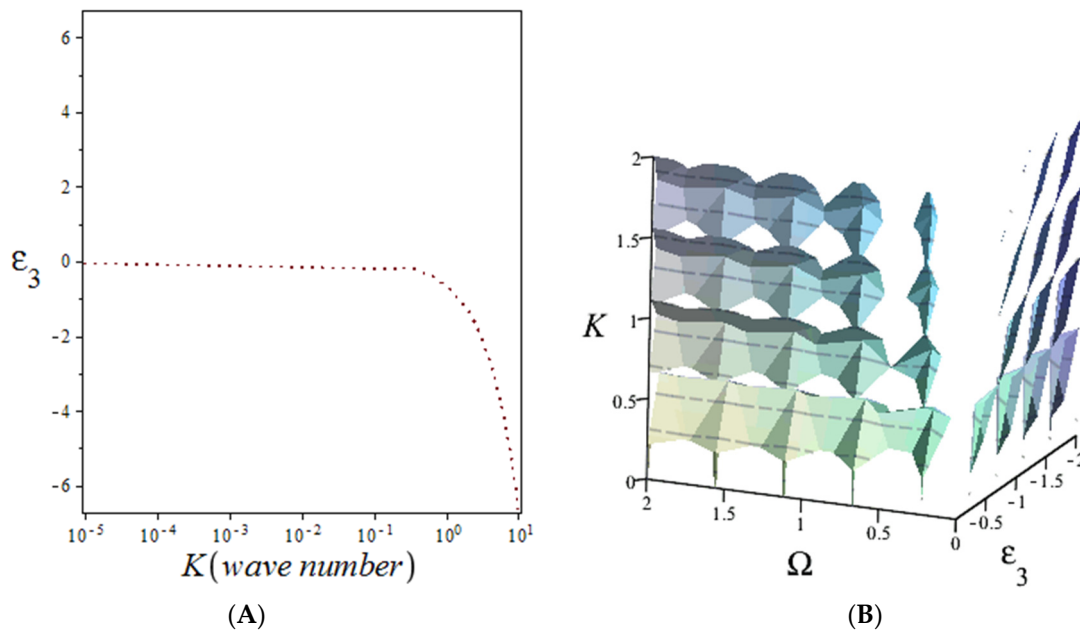(A)　　　　　　　　　　　　　　　　　　　　　　　　　(B)

Figure 9. (**A**) Neutral curves for ε_3 versus the wave number b in the presence of rotation ($\Omega = 10$), and (**B**) three-dimensional view of the critical hypersurface shown in the wave number range $0 \leq K \leq 2$.

8. Conclusions

In this study, a novel model with three parameters (i.e., thermal memories, rotation, and initial stress) was used to examine the photo-thermoelastic behavior of semiconductor waves. The enhanced photo-thermoelastic theory that was taken into consideration was built on the Moore–Gibson–Thompson equation. The heat equation was derived using the Lord–Shulman (LS) thermoelastic model, which served as the starting point. A mathematical physical model of a silicon semiconductor medium was developed. The findings of our study showed that the fundamental factors—in particular, the thermal relaxation times, rotation parameters, and initial stress—had a significant impact on the photothermal behavior of the major physical fields. The quantitative information leads us to the conclusion that the thermal relaxation time decreases the mechanical and thermo-optical waves along the axes. As the x-axis (distance) moves toward infinity, all functions trend to zero, indicating the vanishing of all components for high values of x. It should also be noted that the medium's rate of rotation affects the complex circular frequency and the wave number, as well as how the waves behave in many physical sectors. Applications that exploit the vibrations of microsensor and microresonator systems can be designed and developed with the help of the physical information offered in this study. Finally, it should be mentioned that the findings of this study are intended to be used as criteria for confirming the results of other mathematical methods and to aid in the design of machines.

Author Contributions: K.L.: Conceptualization, Methodology, Supervision; M.A.S.: Software, Data Curation; W.S.H.: Validation, Writing—Original Draft Preparation; A.E.-D.: Visualization, Investigation; R.C.: Software, Writing—Review and Editing. All authors have read and agreed to the published version of the manuscript.

References

1. Biot, M.A. Thermoclasticity and irreversible thermodynamics. *J. Appl. Phys.* **1956**, *27*, 240–253. [CrossRef]
2. Lord, H.; Shulman, Y. A generalized dynamical theory of thermoelasticity. *J. Mech. Phys. Solids.* **1967**, *15*, 299–309. [CrossRef]
3. Green, A.E.; Lindsay, K.A. Thermoelasticity. *J. Elast.* **1972**, *2*, 1–7. [CrossRef]
4. Chandrasekharaiah, D.S. Thermoelasticity with second sound: A review. *Appl. Mech. Rev.* **1986**, *39*, 355–376. [CrossRef]
5. Chandrasekharaiah, D.S. Hyperbolic thermoelasicity: A review of recent literature. *Appl. Mech. Rev.* **1998**, *51*, 705–729. [CrossRef]
6. JSharma, N.; Kumar, V.; Dayal, C. Reflection of generalized thermoelastic waves from the boundary of a half-space. *J. Therm. Stresses.* **2003**, *26*, 925–942. [CrossRef]
7. Gordon, J.P.; Leite, R.C.C.; Moore, R.S.; Porto, S.P.S.; Whinnery, J.R. Long-transient effects in lasers with inserted liquid samples. *Bull. Am. Phys. Soc.* **1964**, *119*, 501. [CrossRef]
8. Kreuzer, L.B. Ultralow gas concentration infrared absorption spectroscopy. *J. Appl. Phys.* **1971**, *42*, 2934. [CrossRef]
9. Tam, A.C. *Ultrasensitive Laser Spectroscopy*; Academic Press: New York, NY, USA, 1983; pp. 1–108.
10. Tam, A.C. Applications of photoacoustic sensing techniques. *Rev. Mod. Phys.* **1986**, *58*, 381. [CrossRef]
11. Tam, A.C. *Photothermal Investigations in Solids and Fluids*; Academic Press: Boston, MA, USA, 1989; pp. 1–33.
12. Todorovic, D.M.; Nikolic, P.M.; Bojicic, A.I. Photoacoustic frequency transmission technique: Electronic deformation mechanism in semiconductors. *J. Appl. Phys.* **1999**, *85*, 7716. [CrossRef]
13. Song, Y.Q.; Todorovic, D.M.; Cretin, B.; Vairac, P. Study on the generalized thermoelastic vibration of the optically excited semiconducting microcantilevers. *Int. J. Solids Struct.* **2010**, *47*, 1871. [CrossRef]
14. Chen, P.J.; Gurtin, M.E.; Williams, W.O. A note on non-simple heat conduction. *ZAMP* **1968**, *19*, 969–970. [CrossRef]
15. Chen, P.J.; Gurtin, M.E.; Williams, W.O. On the thermodynamics of non- simple elastic materials with two temperatures. *ZAMP* **1969**, *20*, 107–112. [CrossRef]
16. Chen, J.K.; Beraun, J.E.; Tham, C.L. Ultrafast thermoelasticity for short-pulse laser heating. *Int. J. Eng. Sci.* **2004**, *42*, 793–807. [CrossRef]
17. Youssef, H.M. Theory of two-temperature-generalized thermoelasticity. *IMA J. Appl. Math.* **2006**, *71*, 383–390. [CrossRef]
18. Youssef, H.M.; Al-Lehaibi, E.A. State-space approach of two-temperature generalized thermoelasticity of one-dimensional problem. *Int. J. Solids Struct.* **2007**, *44*, 1550–1562. [CrossRef]

19. Youssef, H.M.; El-Bary, A.A. Mathematical model for thermal shock problem of a generalized thermoelastic layered composite material with variable thermal conductivity. *Math. Probl. Eng.* **2006**, *12*, 165–171. [CrossRef]
20. Quintanilla, T.Q.; Tien, C.L. Heat transfer mechanism during short-pulse laser heating of metals. *ASME J. Heat Transf.* **1993**, *115*, 835–841.
21. Abbas, I. A two-dimensional problem for a fibre-reinforced anisotropic thermoelastic half-space with energy dissipation. *Sadhana* **2011**, *36*, 411–423. [CrossRef]
22. Quintanilla, R. Moore-Gibson-Thompson thermoelasticity. *Math. Mech. Solids* **2019**, *24*, 4020–4031. [CrossRef]
23. Quintanilla, R. Moore-Gibson-Thompson thermoelasticity with two temperatures. *Appl. Eng. Sci.* **2020**, *1*, 100006. [CrossRef]
24. Aboueregal, A.; Sedighi, H.; Shirazi, A.; Malikan, M.; Eremeyev, V. Computational analysis of an infinite magnetothermoelastic solid periodically dispersed with varying heat flow based on non-local Moore–Gibson–Thompson approach. *Contin. Mech. Thermodyn.* **2022**, *34*, 1067–1085. [CrossRef]
25. Abouelregal, A.; Ersoy, H.; Civalek, Ö. Solution of Moore–Gibson Thompson equation of an unbounded medium with cylindrical hole. *Mathematics* **2021**, *9*, 1536. [CrossRef]
26. Marin, M.; Öchsner, A.; Bhatti, M. Some results in Moore-GibsonThompson thermoelasticity of dipolar bodies. *J. Appl. Math. Mech.* **2020**, *100*, e202000090. [CrossRef]
27. Abouelregal, A.; Marin, M.; Askar, S. Thermo-optical mechanical waves in a rotating solid semiconductor sphere using the improved Green–NaghdiIII model. *Mathematics* **2021**, *9*, 2902. [CrossRef]
28. Abbas, I. Generalized magneto-thermoelasticity in a nonhomogeneous isotropic hollow cylinder using the finite element method. *Arch Appl. Mech.* **2009**, *79*, 41–50. [CrossRef]
29. Lotfy, K.; Seddeek, M.; Hassanin, W.; El-Dali, A. Analytical Solutions of Photo-Generated Moore–Gibson–Thompson Model with Stability in Thermoelastic Semiconductor Excited Material. *Silicon* **2022**. [CrossRef]
30. Mandelis, A.; Nestoros, M.; Christofides, C. Thermoelectronic-wave coupling in laser photothermal theory of semiconductors at elevated temperature. *Opt. Eng.* **1997**, *36*, 459. [CrossRef]
31. Todorovic, D.M. Plasma, thermal, and elastic waves in semiconductors. *Rev. Sci. Instrum.* **2003**, *74*, 582. [CrossRef]
32. Vasil'ev, A.N.; Sandomirskii, V.B. Photoacoustic effects in finite semiconductors. *Sov. Phys. Semicond.* **1984**, *18*, 1095.
33. Christofides, C.; Othonos, A.; Loizidou, E. Influence of temperature and modulation frequency on the thermal activation coupling term in laser photothermal theory. *J. Appl. Phys.* **2002**, *92*, 1280. [CrossRef]
34. Song, Y.Q.; Bai, J.T.; Ren, Z.Y. Study on the reflection of photothermal waves in a semiconducting medium under generalized thermoelastic theory. *Acta Mech.* **2012**, *223*, 1545. [CrossRef]
35. Aldwoah, K.A.; Lotfy, K.; Mhemdi, A.; El-Bary, A. A novel magneto-photo-elasto-thermodiffusion electrons-holes model of excited semiconductor. *Case Stud. Therm. Eng.* **2022**, *32*, 101877. [CrossRef]
36. Alhejaili, W.; Lotfy, K.; El-Bary, A. Photo–elasto–thermodiffusion waves of semiconductor with ramp-type heating for electrons–holes-coupled model with initial stress. *Waves Random Complex Media* **2022**. [CrossRef]
37. Xiao, Y.; Shen, C.; Zhang, W.B. Screening and prediction of metal-doped α-borophene monolayer for nitric oxide elimination. *Mater. Today Chem.* **2022**, *25*, 100958. [CrossRef]
38. Liu, J.; Han, M.; Wang, R.; Xu, S.; Wang, X. Photothermal phenomenon: Extended ideas for thermophysical properties characterization. *J. Appl. Phys.* **2022**, *131*, 065107. [CrossRef]
39. Abbas, I. A GN model for thermoelastic interaction in an unbounded fiber-reinforced anisotropic medium with a circular hole. *Appl Math Lett.* **2013**, *26*, 232–239. [CrossRef]
40. Abbas, I. Eigenvalue approach on fractional order theory of thermoelastic diffusion problem for an infinite elastic medium with a spherical cavity. *Appl. Math. Model.* **2015**, *39*, 6196–6206. [CrossRef]
41. Abbas, I.; Abdalla, A.; Alzahrani, F.; Spagnuolo, M. Wave propagation in a generalized thermoelastic plate using eigenvalue approach. *J. Therm. Stress.* **2016**, *39*, 1367–1377. [CrossRef]